

Performance Evaluation of a Wearable Tattoo Electrode Suitable for High-Resolution Surface Electromyogram Recording

Sourav Chandra , Jinghua Li, Babak Afsharipour , *Member, IEEE*, Andres F. Cardona, Nina L. Suresh, Limei Tian , Yujun Deng, Yishan Zhong, Zhaoqian Xie , Haixu Shen , Yonggang Huang, John A. Rogers, *Fellow, IEEE*, and William Z. Rymer , *Life Member, IEEE*

Abstract—Objective: High-density surface electromyography (HD-sEMG) has been utilized extensively in neuromuscular research. Despite its potential advantages, limitations in electrode design have largely prevented widespread acceptance of the technology. Commercial electrodes have limited spatial fidelity, because of a lack of sharpness of the signal, and variable signal stability. We demonstrate here a novel tattoo electrode that addresses these issues. Our dry HD electrode grid exhibits remarkable deformability which ensures superior conformity with the skin surface, while faithfully recording signals during different levels of muscle contraction. Method: We fabricated a 4 cm×3 cm tattoo HD electrode grid on a stretchable electronics membrane for sEMG applications. The grid was placed on the skin overlying the biceps brachii of healthy subjects, and was used to record signals for several hours while tracking different isometric contractions. Results: The sEMG signals were recorded successfully from all 64 electrodes across the grid. These electrodes were able to faithfully record sEMG signals during repeated contractions while maintaining a stable baseline at rest. During voluntary contractions, broad EMG frequency

Manuscript received August 28, 2019; revised February 17, 2020, June 20, 2020, August 24, 2020, and October 1, 2020; accepted October 10, 2020. Date of publication October 20, 2020; date of current version March 19, 2021. This work was supported by the Shirley Ryan Ability Lab, and Northwestern University. The Work of Sourav Chandra was supported by NIDILRR ARRT grants. The work of Jinghua Li was supported by the startup funds of The Ohio State University. The work of Andres F. Cardona and Nina Suresh was supported by NIH-RO1 (5RO1HD089952). The work of Zhaoqian Xie was supported by the National Natural Science Foundation of China under Grant 12072057 and Fundamental Research Funds for the Central Universities under Grant DUT20RC(3)032. The work of Yonggang Huang was supported by NSF under Grant CMMI1635443. (Sourav Chandra and Jinghua Li contributed equally to this work.) (Corresponding author: William Z. Rymer.)

Sourav Chandra, Nina L. Suresh, Yujun Deng, Haixu Shen, Yonggang Huang, and John A. Rogers are with the Northwestern University and also with the Shirley Ryan Ability Lab,.

Jinghua Li is with the Northwestern University, and also with the Ohio State University.

Babak Afsharipour is with the University of Alberta.

Andres F. Cardona is with the Shirley Ryan Ability Lab.

Yishan Zhong is with the University of Illinois Urbana Champaign.

Limei Tian is with the Texas A&M University.

Zhaoqian Xie is with the Dalian University of Technology.

William Z. Rymer is with the Northwestern University, Chicago, IL 60611-2654 USA and also with the Shirley Ryan Ability Lab (e-mail: w-rymer@northwestern.edu).

Digital Object Identifier 10.1109/TBME.2020.3032354

content was preserved, with accurate reproduction of the EMG spectrum across the full signal bandwidth. *Conclusion:* The tattoo grid electrode can potentially be used for recording high-density sEMG from skin overlying major limb muscles. Layout programmability, good signal quality, excellent baseline stability, and easy wearability make this electrode a potentially valuable component of future HD electrode grid applications. *Significance:* The tattoo electrode can facilitate high fidelity recording in clinical applications such as tracking the evolution and time-course of challenging neuromuscular degenerative disorders.

Index Terms—HD-sEMG, tattoo electrode, stretchable electronics, wearable electrode.

I. INTRODUCTION

▼ IGH-DENSITY electrode grids have multiple potentially IGH-DENSITY electrone grown many many many unique applications for recording myoelectric activity from a specific muscle or muscle group, and often provide exclusive information compared to other sEMG recording modalities [1]. The primary attraction of the high-density (HD) grid is linked both to its noninvasive nature and to its capability to record from a large area over the muscle surface. These features help to capture reliable information about muscle activity and extract information about peripheral and central properties of neuromuscular systems [2]. Recording neuromuscular activation at high spatiotemporal resolution using a noninvasive surface grid possesses a number of major advantages for neuroscience and human motor control research. The HD-sEMG recordings play a useful role in issues like evaluating the conduction velocities of muscle fibers, locating the muscle innervation zone, identifying EMG interference patterns, understanding the spatial distribution of muscle fiber action potentials, and quantifying the spatio-temporal distribution of MUAP firing patterns in a noninvasive manner [3]–[5]. Long-term accurate recordings of muscular activity can also be greatly enhanced by a wearable HD electrode grid [6]–[8].

In addition to their potential importance in basic neuromuscular research, these types of grid electrodes may also help in early diagnosis and tracking of several disabling neuromuscular diseases such as Spinal Muscular Atrophy (SMA), and Amyotrophic Lateral Sclerosis (ALS) [1], [9]. Whilst many HD-sEMG recordings claim to provide detailed neuromuscular information, electrode layout configurability and prolonged wearability without compromising skin-electrode interface environment (by limiting variation of the moisture content at the interface) remain as major challenges for these grid electrodes [10]. The "skin-electrode interface environment "refers to the space between the skin and the electrode grid which is critical for both long-term wearability and accuracy in EMG signal measurement. To illustrate, it was reported that trapped moisture at the interface between thick silicon film (1 mm) and skin can result in irritation [11].

Earlier experimental studies have demonstrated the utility of a thin structured flexible electrode for recording facial muscle activity successfully [8] and for recording from a smaller peripheral muscle (such as the first dorsal interosseous (FDI)) [12]. The flexible grid was shown to achieve an acceptable high-density layout. However, skin conformity becomes less secure in the peripheral electrodes of the grid such that the outer columns/rows often become unusable [7], [13].

Recently, a screen printing process has been used to design sEMG electrodes to improve skin conformity [2]. A major reported drawback of such printed electrodes has been their poor electrical and mechanical properties; these may be adversely affected by fluctuations of regional moisture content at the electrode skin interface. This moisture often degrades signal reliability over time [2]. Several other approaches using printed carbon electrode grids have also acknowledged the problem of rapid aging, dimensional instability and significant changes in electrode conductance over time [14], [15].

Layout programmability is a challenging but important design feature of the HD-sEMG grids. Increasing the number of electrodes, with reduced electrode diameter and inter-electrode distance is preferred for single motor unit discrimination, as it provides the ability to record a sharper signal with greater functional details. These grid recording properties may thus help accurate quantification of muscle activity [16] and facilitate accurate MU decomposition analyses [17].

Despite these promising diagnostic and research applications, commercially available sEMG grid electrodes routinely exhibit technical barriers that limit construction of dense layout configurations, and impact the quality of HD-sEMG recordings, due to limitations of their mechanical and material properties [12]. Current limitations include membrane "stretchability", adequate skin conformity and overall wearability. The potentially promising advantages of grid layout configurability are therefore largely lost, since a majority of the electrode designs do not allow the user to choose the height, electrode diameter, inter-electrode distance, and the overall layout. To overcome these limitations, we here describe design features that allow us to optimize electrode designs for effective recordings in human subjects. Our major challenge is to be able to provide stable, high spatial resolution, better signal to noise ratio (SNR) recordings of surface electromyogram (sEMG) signals from a reconfigurable and easy wearable grid electrode.

In this paper, we describe the feasibility, advantages, and signal recording performance of a novel HD grid electrode, designed specifically for sEMG applications. We call it a "tattoo" because of its light-weight and stick-on, malleable characteristics. The tattoo electrode grid is extremely flexible in nature, built on stretchable electronics [18] specifically designed and structurally optimized for the sEMG application with programmability option for the electrode layout within the grid. This provides the flexibility of controllable electrode dimensions,

inter-electrode distance, and the grid montage with micron-level accuracy [19], [11]. These electrodes can record while being dry (no gel/paste), which makes them more suitable for stable long-term recording [20].

We report here on tattoo based recordings from the human Biceps Brachii (BB) muscles in a laboratory setup. We have also compared the properties of the sEMG signal acquired through the tattoo electrode with recordings from a commercial grid electrode (TMSI). Finally, we present preliminary guidelines for using such a tattoo electrode in several sEMG applications.

II. DEVICE FABRICATION AND MATERIAL DESCRIPTION

The schematic illustration and design of the device appear in Fig. 1. (a)–(c) To achieve larger elastic stretchability, finite element analysis (FEA) is used to optimize the center angle θ and the width W of the serpentine wire, as shown in Fig. 1(c) (right). Here the strain in the Au layer should be less than the yield strain of 0.3%. The elastic stretchability of the serpentine wire with θ = 270° and W = 900 μ m can reach ~37% (Fig. 1(d)). Fig. 1(e) highlights the elastic stretchability of the device deployed on the skin surface, as a function of the width and center angle of the serpentine wire, emphasizing the programmability of the electrode grid layouts when guided by theoretical modeling.

Each device described here consists of 64 Au mesh electrodes (thickness: 300 nm, diameter: 1mm, fill factor: 50%) connected by serpentine wires and anisotropic conductive film to external data-acquisition systems. The mesh electrodes make direct contact with the skin surfaces. Polyimide (PI) encapsulates the gold interconnect wires for electrical insulation. The encapsulation also places the wires into the mechanical neutral plane to maximize grid flexibility and stretchability. Microperforated soft silicone serves as a breathable substrate with cross-linked adhesive silicone to form the robust skin-electrode interface.

Fabrication of epidermal electronics for the tattoo grid begins with spin coating of a thin layer of polydimethylsiloxane (PDMS, 10 μ m, Dow Corning. Inc.) on a glass slide, followed by treatment using oxygen plasma. Spin coating of a thin layer of PI (spin speed: 3000 RPM, 2 μ m) and subsequent curing at 350°C yields the bottom encapsulation layer. Electron-beam evaporation of gold film (300 nm), photolithography and etching then define conductive traces with serpentine structure, all designed using FEA. Here FEA is used to simulate the mechanics of the mesh electrode arrays mounted on the substrate and laminated on the skin. The stretchability refers to the point where the Au layer exceeds its yield strain (0.3%) across half of the width of any section. The results provide information on the elastic stretchability of devices with varied structural parameters such as the width and angle of the wires, in order to accommodate the natural deformations of the skin. FEA enables the design of the structural layout in a tunable and programmable fashion to meet the requirement for targeted applications with a specific stretchability. Another layer of PI (2 μ m) patterned by photolithography and oxygen plasma etching creates the top encapsulation layer to place the electrodes into the mechanical neutral plane. Spin coating of a layer of Ecoflex $^{\mathrm{TM}}$ (8 $\mu \mathrm{m}$, Smooth-On. Inc.) and the second layer of adhesive silicone (80 μ m; RT GEL 4642, Bluestar. Inc.) forms a self-adhesive surface on a thin Polyethylene Terephthalate (PET) sheet (50 μ m; Grafix DURA-LAR). A PDMS stamp transfers a monolayer

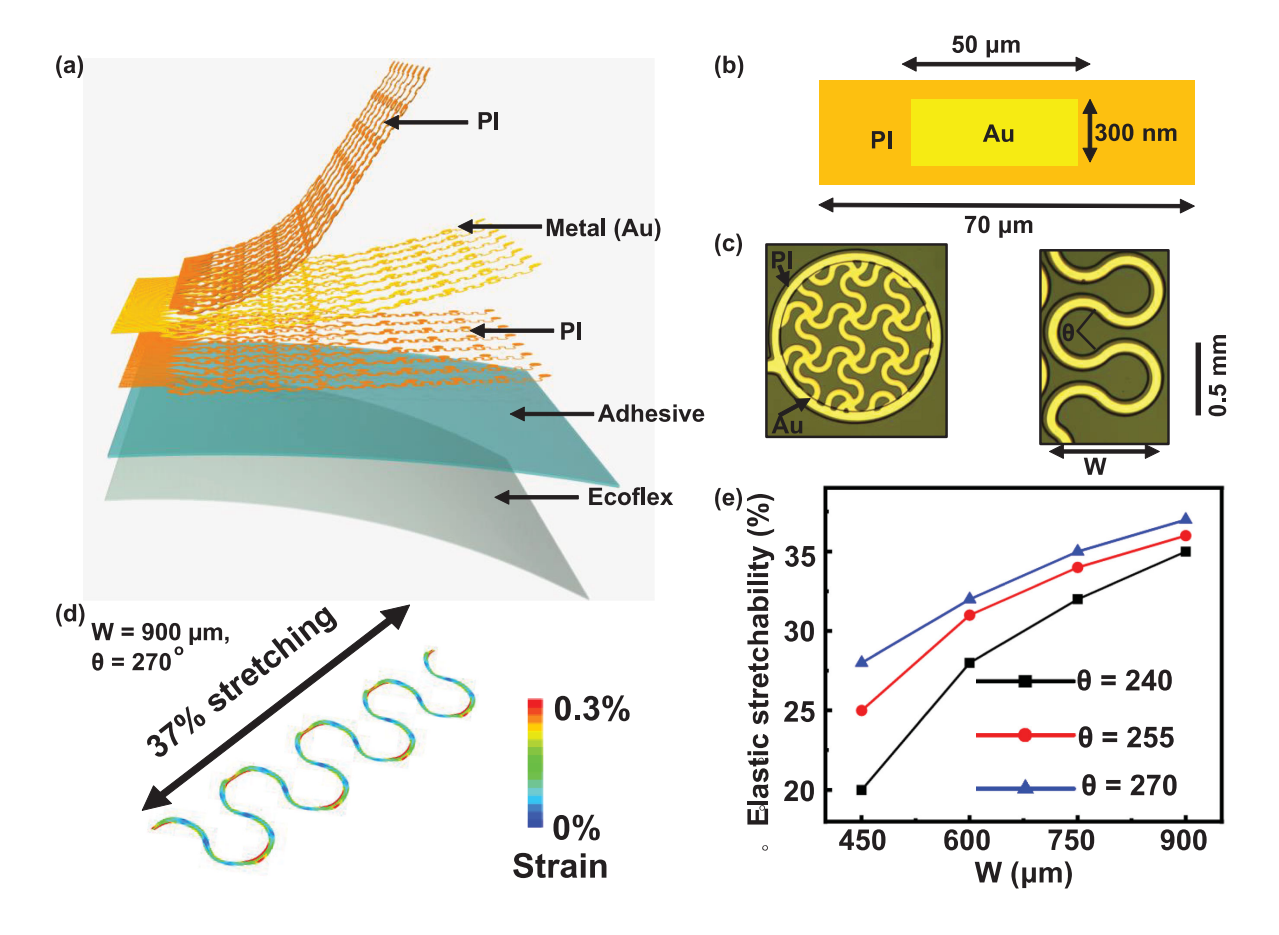


Fig. 1. (a) Exploded-view schematic illustration of key functional layers of the 64-channel epidermal electronics. PI layers encapsulate the Au traces from the environment and also provide mechanical support. (b) Cross-sectional illustration of the epidermal electronics. (c) Optical images of a mesh electrode (left, fill factor: 50%) and a serpentine wire (right) on the adhesive silicone surface. (d) Computational results by finite element analysis that indicate large elastic stretchability of ~37% in a serpentine wire. (e) Simulated stretchability of the device on skin surface as a function of the width and central angle of the serpentine wire showing the programmability of this technology.

of poly (methyl methacrylate) microspheres on the surface of the adhesive layer. Thermal curing followed by dissolving the microspheres in acetone forms the porous adhesive interface. A water-soluble cellulose tape (3M Inc.) retrieves the fabricated electrodes from the rigid glass substrate. Attaching the tape to the adhesive silicone surface on PET enables the transfer of the electrode to the flexible substrate (Fig. 1(a)–(c)). Dissolving the water-soluble tape completes the preparation of the tattoo

A thin anisotropic conductive cable (HST-9805-210, Elform Inc.) is then bonded to contacting pads of the devices with heat and pressure to connect to the back-end data-acquisition system.

a Magnitude (dB) Impedance (1mm 1mm 10mm 10 10¹ Frequency (Hz) Frequency (Hz) (b)

140

(a) Electrical impedance of mesh electrodes (fill factor: 50%) with different diameters (1 mm, 2.5 and 10 mm). The individual data points represent the averages of three measurements. (b) Estimated Bode amplitude response of the respective electrode.

III. EXPERIMENTAL DETAILS

A. Experimental Characterization of the Electrode

Fig. 2(a) shows the measurements using electrochemical impedance spectroscopy (EIS) to evaluate the quality of the mesh electrodes reported in this work, with diameter of 2.5, 10 mm (fill factor: 50%), and estimated response of 1mm diameter (green trace in Fig. 2(a), (b) respectively based on our previous work [11]. During the EIS measurement, a pair of tattoo electrodes served as a working and as a reference electrode, respectively. A commercial gel electrode of 1 cm² was used as a counter electrode. The impedance was measured over the frequency range from 1 to 1000 Hz, values highly relevant to surface EMG signals, which lie in the frequency range from 0 to 500 Hz and are most dominant in between 50-150 Hz [21]. The impedance increases with decreasing electrode diameter due to a decrease in the effective skin-electrode contact area. These results enable a comparison with the impedance of the commercial electrodes reported in literature.

For example, a mesh electrode of this type with the same material (300 nm Au, diameter: 10 mm, fill factor 50%, effective contact area: 0.39 cm²) shows an impedance value of \sim 500 k Ω

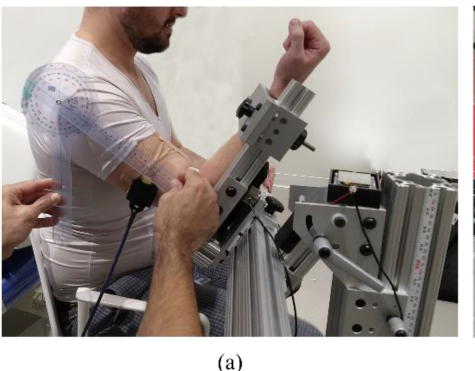




Fig. 3. (a) The experimental setup with the elbow torque measurement device. (b) The tattoo electrode placed on the skin surface of biceps brachii muscle with the connecting wire and the connector board of the tattoo electrode.

at 10 Hz and $\sim 80~\text{k}\Omega$ at 500 Hz. These values are comparable to those reported for commercial gel electrodes (effective contact area: 1 cm², $\sim 200~\text{k}\Omega$ at 10 Hz and $\sim 30~\text{k}\Omega$ at 500 Hz) [22], a finding consistent with the conclusion in our previous study [23]. Fig. 2(b) shows the Bode plot amplitude response for the electrode, based on the estimated value from the response 2(a).

B. Experimental Methods

We studied three intact individuals during isometric elbow contractions while recording the sEMG from the primary elbow flexor muscle, the biceps brachii. Our subjects had no prior history of neurological illness and provided informed consent. Consents were obtained from the participants in accordance with Helsinki Declaration of 1975, revised in 2000.

Subjects were seated on a chair and their forearm was attached via a rigid link to a multi-axial load cell mounted at the wrist, as shown in Fig. 3(a). All sEMG electrode data were collected with the tattoo electrode and with a commercial bio-amplifier (TMSI. Inc. RefaTM 128) in parallel with recordings of elbow joint torques. The tattoo was connected to the amplifier with a thin film bus and a lock-in connector (Fig. 3(b)).

For our electrode layout, we used a rectangular grid of 4 cm×3 cm area encompassing a total of 64 electrodes with 4 mm inter-electrode distance and 1 mm electrode diameter. The grid, being extremely flexible, ensures a malleable skin interface that conforms with BB's shape, both during muscle contraction and during rest. All sixty-four tattoo channels were recorded concurrently, using a common reference measurement topology. A reference electrode (dimension of 8mm×8mm) was manufactured from the same material as the electrode and was placed on the acromion during the recording.

To compare the tattoo electrode performance with conventional surface grid electrodes, we also recorded sEMG at the same contraction levels with a commercially available sEMG grid electrode (TMSI Inc.) with 3 cm \times 3 cm electrode surface area, 4 mm inter-electrode distances and 2mm electrode diameters. An identical experimental protocol (to the tattoo) was followed with the same subject and in the same experimental setup.

Surface electrodes can be characterized by physical dimension, shape, size, electrode material, and underlying technology.

For a given electrode interface the resistance offered by the electrode is estimated from $R = \rho L/A$. Where R is the resistance offered, L is the thickness of the printed electrode, A is the area of the electrode and ρ is the resistivity of the material. We have retained a standard circular shape, with the consistent electrode area (1 mm diameter) and thickness for all our experimental trials during these experiments. The density of the filling material in the pattern was also maintained constant.

C. Skin Preparation

The tattoo electrode requires a relatively mild skin preparation (i.e., with alcohol wetted swab), and modest exfoliation, comparable to other commercial grid electrodes. An advantage of the dry tattoo grid is that it does not require any conductive gel/cream to be applied to the area, and thus it does not require the user to apply separate skin adhesive tapes, like other electrodes [8], [7], [24]. With the process of skin preparation shortened, the electrode placement is easier, faster, and convenient for the subject, with minimum discomfort.

D. Skin Electrode Attachment and Connection

After thorough skin preparation, and after identifying the boundaries of the BB muscle, the tattoo grid was mounted on the skin surface over the biceps brachii muscle. The electrode had an inbuilt biocompatible non-irritating microporous silicone adhesive on the sticking skin surface. The transparent adhesive layer (Fig. 1(a)), helps the grid to securely stick to the skin. The adhesive layer is a commercial product that is electrically insulating. It is used to provide sufficient strength to form a robust skin-electrode interface.

To preserve the consistency of electrode grid placement across recording sessions, we recorded the boundaries of the grid location on the skin for each participant, using bony landmark references, such as the acromion, the cubital fossa boundaries, as well as the medial and lateral epicondyles of the humerus. We could then place the electrode in the same location in different sessions with millimeter level accuracy. To improve our placement accuracy, we also traced the grid boundary on the skin with a surgical marker pen, and recorded the grid center and corners to aid accurate positioning.

E. The Electrode Connector

The electrodes were connected to the amplifier system via serpentine connectors within the grid layout. The internal serpentine connector was also structurally flexible to conform with the curved skin surface, that routinely changes shape during contraction. These serpentines were routed to a flexible lightweight 64 channel connector bus insulated with the same grid base material (PI) as shown in Fig. 3(b). The connectors offer the necessary flexibility to stay on the skin for a long time period without deforming the electrode or the connecting wire.

A soft, flexible flat ribbon bus connector was then used, that generated minimal movement artifact during muscle contraction. The signal bus was connected to an amplifier board through a specially designed modular PCB connector. The connector with a click-in attachment ensured a secure connection during the signal acquisition.

F. The Amplifier

A 128 channel TMSI Refa HDEMG amplifier (TMSI. Inc.) was used for data acquisition. Channels 1-64 actively acquired signals, while channels 65-128 were disabled. The signal acquisition system has high input impedance (>1 G Ω) and high CMRR (>120 dB). All channel signals were first amplified in a monopolar configuration (Gain = 26.5). Signals were then digitized with 24-bit resolution at a rate of 2000 samples/second in each channel individually. The acquisition software (PortiLab $^{\rm TM}$) allowed a channel-by-channel visual inspection of the signal during the acquisition. Bad channels acquiring noisy data were automatically rejected by the acquisition software. The digitized signals were then stored in a solid-state memory through a personal computer.

G. Recording Modality

Grid EMG signals were recorded in a monopolar mode with a reference electrode placed on the acromion of the subject. A second electrode placed at the lateral epicondyle was used to improve the EMG signal by actively reducing the common-mode components during the recording. The ground electrodes were 4mm×4mm area and square in shape, secured with adhesive to the skin.

H. Experimental Protocol

Voluntary sEMG signals were recorded during a sustained isometric non-fatiguing elbow flexion task. To begin, a maximum voluntary contraction (MVC) trial was performed, and this was followed by four submaximal contraction trials (at 30%, 60%) of the recorded MVC. We set a time gap of two minutes between each trial to minimize muscle fatigue. Subjects were queried repeatedly regarding systemic as well as muscle fatigue before beginning of each trial. The targeted contraction force trajectory was trapezoidal in nature, with programmed torque trajectory increasing at 10% of the target force/s, reaching steady-state (with epoch duration of 10 seconds) and then decreasing with a symmetric declining torque request. A visual display of the desired trajectory in a quadrant plane, along with auditory feedback was provided to help the participants track their force profile as required.

I. Recording Procedure

The subject was instructed to sit in an upright position on a Biodex chair (Biodex. Inc.). Sitting posture and joint angles were maintained constant during different recording episodes. The arm position, the elbow and shoulder flexion, shoulder abduction, and forearm pronation angles were also kept constant. Subjects were instructed to sit in a relaxed position first for baseline recording (Fig. 3(a)). A Maximum Voluntary Contraction (MVC) trial was then performed followed by a sequence of graded submaximal contractions. The elbow contraction force was recorded with a 6 DOF force-torque sensor (ATI. Inc.), and a visual tracking display was provided to the subject for accurate reproduction of the desired contraction force level during the trial. Each trial sequence lasted about 2 hours. A "rest" trial was recorded at the end of the 2-hour session to compare the final

baseline signal quality with the initial recordings, to assess long term wearability.

J. Data Analysis

For each recorded channel, signals were processed by performing signal mean removal, bandpass digital filtering (5Hz-400 Hz, FIR, 4th order), and power line interference removal based on spectral line interpolation [25]. Trials with motion artifacts were rejected using strict criteria [27], [29], [24], [30]. The digitized signal was then used for multiple offline analyses.

The baseline root means square (RMS) value was calculated [26] for estimating the noise magnitude at the beginning and the end of the experiment. The RMS value during the activity period was also calculated to quantify the detected activity and to compare with the baseline during the resting state. Both time domain and frequency domain properties were then quantified and compared between the tattoo and the commercial TMSI electrodes.

Though clinical applications of the sEMG do not currently utilize much of the available frequency domain information, this information is still extremely useful to help assess the performance of the electrodes. While analyzing the frequency domain response of the signal, detection and exclusion of those trials contaminated by artifacts due to movement or attributable to motion of the connector PCB were performed with visual screening.

Surface EMG signal peaks were detected from the raw signals recorded from both heads of the biceps brachii muscle. The peaks were estimated from a 1-second window in the sEMG signal during the steady-state period of the trapezoidal force trajectory. In order to select the peaks, a defined threshold was established above which all the peaks were considered for the analysis. The threshold $E_{\rm TH}$ was defined as:

$$E_{TH} = \mu + 3\delta$$

Where μ and δ are the mean and the standard deviation of the baseline signals before the start of the voluntary activation [27]. Finally, both positive and negative peak values of the monopolar signal were recorded, and the total number of peaks was calculated as the sum of all positive and negative peaks. We used Wilcoxon Signed Rank test to check the statistical significance (significance level 0.05). All signal processing was performed with a commercial mathematical package (Matlab $^{\rm TM}$, Math-Works, Inc.).

IV. RESULTS

A. Active and Resting Level Signals

The primary aim of our experiment was to characterize the acquired signal properties and to compare signal quality and characteristics between two different electrode systems. Fig. 4 shows a data subset, using three columns of the grid, and the associated monopolar sEMG signal recorded from biceps brachii during a short contraction followed by rest. The orientation of the column was approximately along the fiber direction of the muscle. The signal baseline recordings were analyzed after recordings were acquired in a post-hoc analysis. The baseline median values of all 64 RMS values recorded from each active

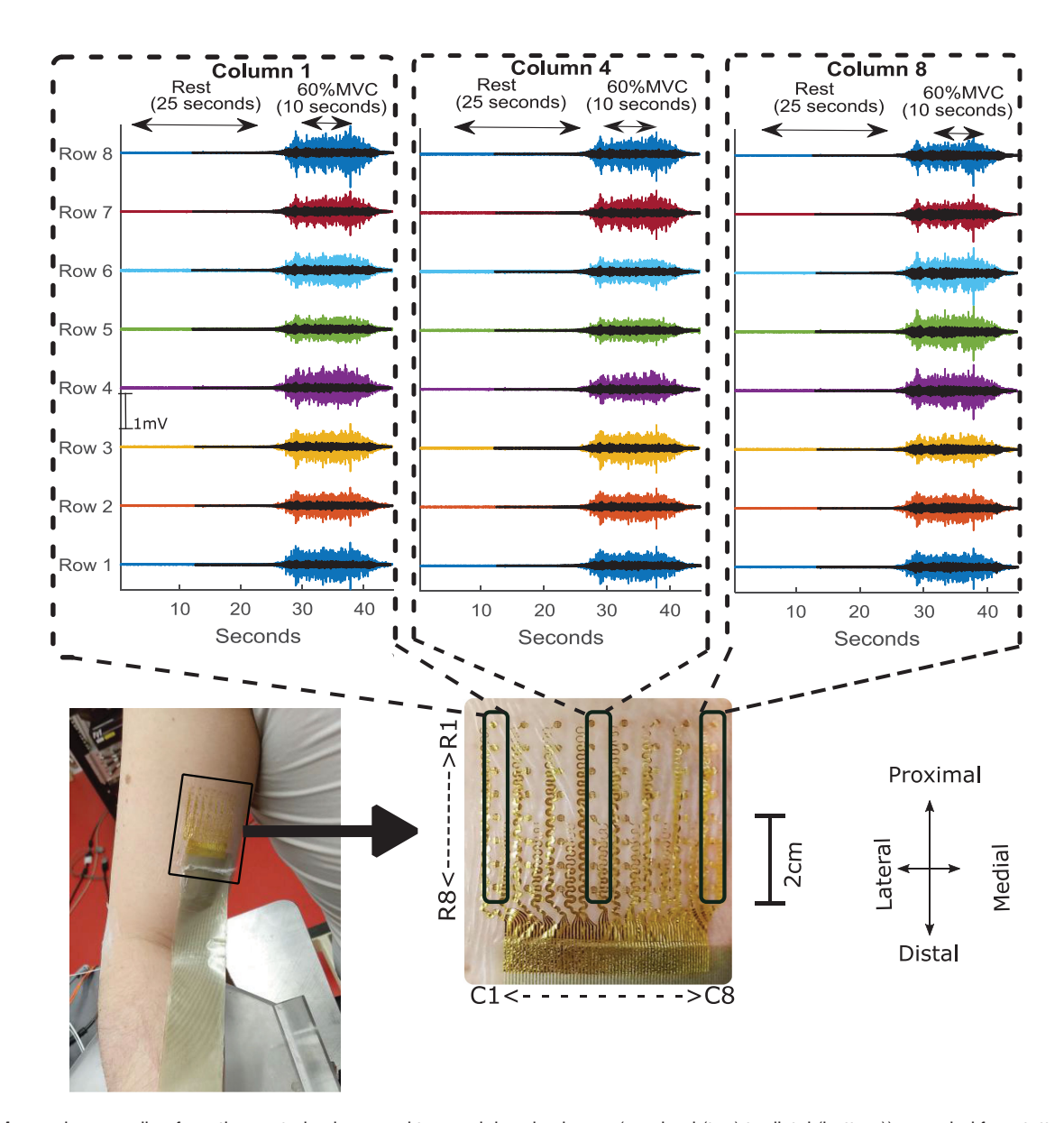


Fig. 4. Monopolar recording from the central column and two peripheral columns (proximal (top) to distal (bottom)) recorded from tattoo electrode (solid color) and commercial electrode (overplayed transparent black color) during resting trials followed by a 60% MVC contraction trial with a trapezoidal trajectory of the force with 10 seconds of steady state contraction. The tattoo location and electrode layout (rows (R) and columns(C)) is shown with a magnified view.

channel were found to be <10 μ V (calculated with 95th percentile) between various contraction level. This analysis showed that the baseline signal was stable for all the channels when the muscle was quiescent. Fig. 5 shows a comparative depiction of the baseline quality of the recorded signal during an isometric contraction trial.

Despite considerable soft tissue movement during contractions, the signal recorded during the onset of high contraction levels was consistently stable, with minimum noise and minimal baseline drift across all the channels, including the most peripheral ones of the grid. The signals acquired during muscle activation were analyzed by calculating the RMS value of the signal from each channel. The values observed in the tattoo electrode recordings were found to be larger compared to the TMSI electrode.

We calculated the ratio between the contraction RMS and the baseline during the resting state. The active signal to baseline ratios during the voluntary contraction trials were then calculated. The calculated values were 46 ± 7 , 40 ± 8 , and 32 ± 7 for the tattoo electrode at 100%, 60%, and 30% MVC contractions respectively. Similarly, the values were also calculated for the TMSI electrodes. The maximum signal to noise value found in the commercial TMSI grid electrode was 30 ± 8 during the MVC while the values for 60%, and 30% MVC contractions were 26 ± 6 and 15 ± 8 .

B. Frequency Domain Properties of the Signal

The frequency-domain responses of both the signal baseline in quiescent muscle, and the active recordings were analyzed after

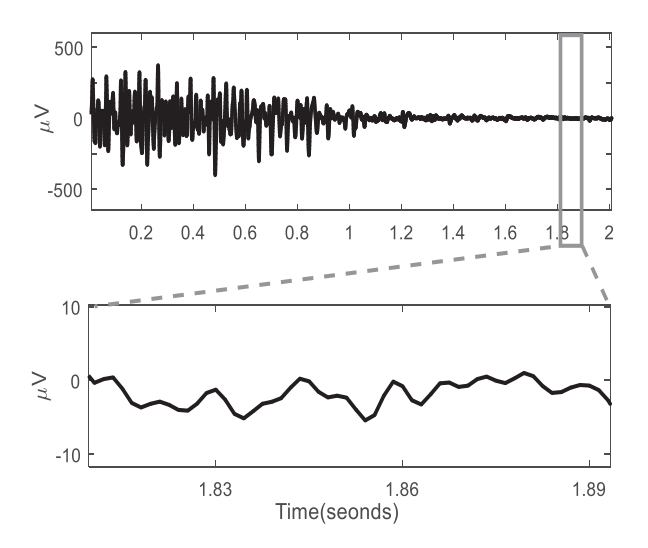


Fig. 5. The sEMG recorded from an electrode channel located in the center (row 4 column 4) during an MVC contraction and the baseline during the relaxation. The signal baseline is plotted with a time scale.

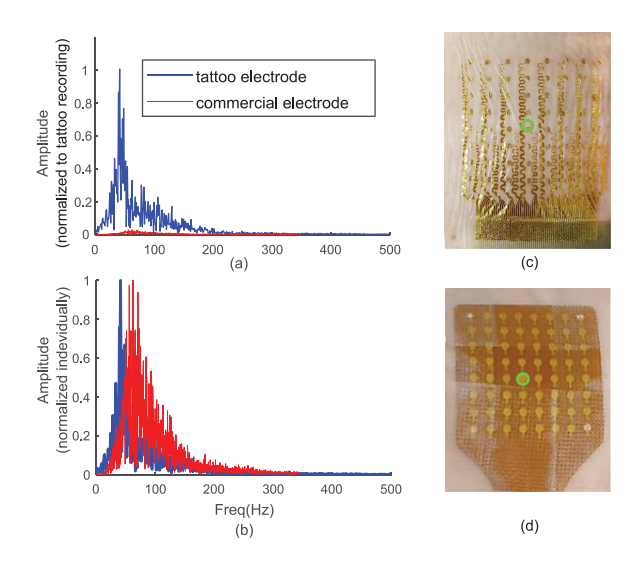


Fig. 6. (a) Frequency response of the sEMG signal recorded during 60% MVC recorded using tattoo electrode (blue) and commercially available electrode (red) normalized to tattoo amplitude. (b) The spectrum normalized to its own maximum for each electrode. The response calculated from the center electrode. (c) The tattoo electrode grid and (d) the commercial electrode with center electrode highlighted with green circle.

Fourier transformation of the signal [28]. The frequency-domain analysis showed that the signal recorded using the dry tattoo electrode had significantly higher frequency content across the relevant spectral range of sEMG during voluntary contraction.

The frequency-domain information of the active region during the 60% MVC contraction recorded in the center channel (4, 4) is presented in Fig. 6(a) and (b). The spectrum calculation was carried out with 1 second (2000 samples) of the signal during the midrange isometric contraction (compared to MVC).

Fig. 6(a) indicates a potential larger frequency response of the tattoo electrode when compared to the commercial electrode. Specifically, the spectrum amplitude for the tattoo electrode was an order of magnitude higher compared to the commercial TMSI electrode. This increase in amplitude was observed across

TABLE I
OCCUPIED BANDWIDTH (ATTRIBUTED TO 99% OF THE TOTAL SIGNAL
SPECTRUM POWER), UPPER FREQUENCY LIMIT (F-HIGH) AND LOWER
FREQUENCY LIMIT (F-LOW) AND THE POWER OF THE RECORDED SIGNAL
RECORDED BY TWO TYPE OF ELECTRODES

MVC Level	Occupied Bandwidth		F-Low (Hz)		F-High (Hz)		Signal Power	
-	Tattoo	Comm.	Tattoo	Comm.	Tattoo	Comm.	Tattoo	Comm.
100%	150±36	170±26	10±2	31±2	160±35	201±24	6±.8×10 ⁸	1.5±.3×10 ⁵
60%	160 ± 29	215±30	7±2	$21{\pm}1$	$167{\pm}28$	$237{\pm}30$	$4.3{\pm}1{\times}10^7$	$3.4{\pm}1.8{\times}10^{4}$
30%	324±43	251±31	18±3	19±1	$305{\pm}21$	$270{\pm}30$	$8.2{\pm}1{\times}10^5$	$9.3 \pm 3.5 \times 10^{3}$
rest	378 ± 19	338 ± 23	10 ± 1	13±1	389±19	352 ± 23	$2\pm0.8\times10^{5}$	$6\pm1\times10^3$

the whole spectrum. The spectrum shape was also preserved across different contraction levels. The normalized amplitude (to maximum value) of the power line frequency in the raw signal were found to be 0.2 ± 0.08 and 0.6 ± 0.036 respectively in the tattoo and in the commercial grid during the 60% MVC trial. During rest, the ratio between the spectral amplitude at powerline frequency and the maximum amplitude in the rest of the spectrum were 5 ± 2.7 in the tattoo and 3.2 ± 2.1 for the commercial electrode. Calculated median and the mean frequencies were 58 ± 6 Hz, 63 ± 9 Hz for the tattoo electrode and 71 ± 12 Hz, 74 ± 14 Hz for the commercial electrode.

In order to understand the sources of the recorded frequency content, we determined the occupied bandwidth (difference in frequency between the points where the integrated power crosses 0.5% and 99.5% of the total power in the spectral response) calculated at different levels of voluntary contraction. These values are summarized in Table I. The occupied bandwidth of the tattoo electrode was found to be comparable to the commercial electrode while the tattoo electrode had a signal power an order of magnitude higher than the TMSI electrode. Higher spectral power was observed during the contractions and these power values were found to be significantly higher (p << 0.1) compared to the commercial electrode.

C. Peak Distribution Analysis

The finding of a significantly higher energy of the signal associated with a comparable occupied bandwidth affirms that larger signal amplitudes were recorded using the tattoo electrode. The peaks in the sEMG signals are often considered to be a representation of the firing characteristic of the motor unit population [29]. The amplitudes of the firing peaks and the distribution of the peak values were analyzed as described in the methods section, to further characterize the signal properties.

The sEMG signal recorded via the dry tattoo showed a greater number of larger peaks detected during a midrange (60%) voluntary isometric contraction activity. The larger amplitudes and greater number of peaks are an indication of more sensitive recording, compared to the commercial sEMG electrode.

As shown in Fig. 7(a), the peaks detected through the dry tattoo electrode were approximately four times larger than the peaks detected by the commercial TMSI grid. In addition to the larger peaks, the number of peaks detected at various force levels was also different (p << 0.01). We have found 931±157, 848±185, 752±218 peaks for maximum, midrange and minimum contraction in the tattoo recording, while the commercial

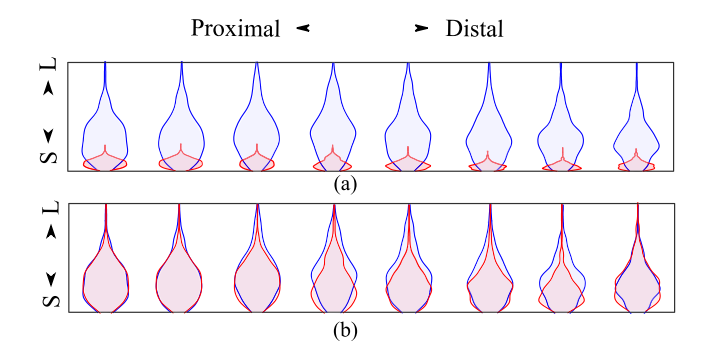


Fig. 7. (a) Distribution of the peaks detected in the central column (column 4) during 60% MVC using tattoo electrode (blue) and commercial electrode (red) from small (S) to large (L). (b) Distribution of peaks normalized to maximum value of the respective electrode channel.

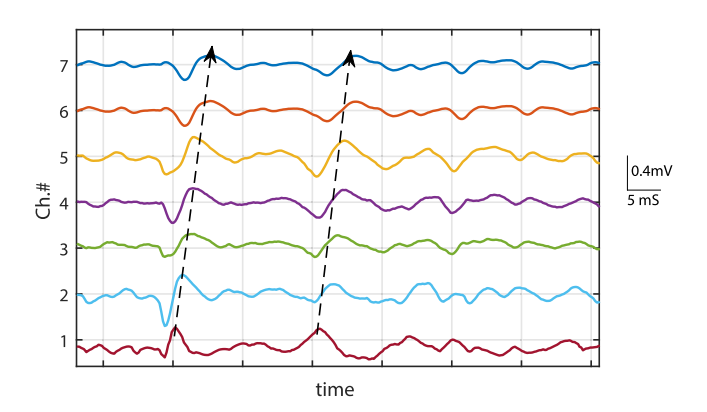


Fig. 8. Propagation of MUAP from voluntary contraction. A short segment of single differential signal from obtained from 8 channels measured along the fiber direction of the biceps brachii muscle. The illustrated arrow indicates the direction of the MUAP propagation.

electrode showed 346 ± 92 , 232 ± 78 and 218 ± 88 peaks for the respective contraction levels.

Fig. 7(b) shows the distribution of the normalized peak amplitudes of the respective grid channel during the midrange isometric elbow contraction task.

The larger range of the sEMG peak distributions also shows a clear trend with additional distribution peaks (Fig. 7(a)) of the sEMG recorded throughout the tattoo grid. This peak distribution shape suggests that additional MUAP details may be accessible, and these recordings will theoretically facilitate MU discrimination from the sEMG.

D. Propagation of Muscle Fiber Action Potentials

To evaluate the topographical properties of action potential propagation in the muscle, the central column of 8 electrodes was selected during 60% MVC contraction trial. Fig. 8 shows the differential of the voltage signals recorded in column 4. The single differential signals between successive monopolar recording channels were calculated offline [24]. The trains of the muscle fiber action potential activity were detected from proximal (plotted in the top) to distal (plotted in the bottom) direction. The action potential train shows a linear time shift along with the electrode array. The direction of the propagation

is visually discernable from the recorded signal trains. The velocity of the propagating MU peaks was used to calculate the conduction velocity of the MUAP on the muscle fiber during the contraction [30]. The value was calculated to be 4.9 m/s in the direction of along the fiber.

V. DISCUSSION

In this study, we illustrate the potential utility of a precisely customizable tattoo grid electrode in a realistic experimental setting. Our study was based on recordings taken directly from human subjects and was intended to examine the potential utility of the tattoo electrode for sEMG recordings. The tattoo electrode recordings showed a high signal-to-noise ratio, large signal amplitude, and faithfully captured MUAP activities, indicating that the grid sEMG signals can potentially be used as a complement to intramuscular needle recordings, at least in some circumstances [1], [2]. We have also studied the electrical performance of the electrode-amplifier system for recording sEMG signal during rest and during voluntary contractions. The tattoo electrode was able to successfully record accurate sEMG signals from all the electrodes across the grid (i.e., for both the center and the peripheral electrodes) during voluntary contractions and during resting conditions. However, we were unable to fully characterize system noise characteristics and other important electrode properties in situ.

We have chosen here a relatively simple tattoo grid layout, with a rectangular shape, to assess recording stability during voluntary muscle contraction. However, in practice, the tattoo grid can be designed to have almost any shape and size needed to match specific muscle contours [11], [20], and thus we demonstrate its potential for a wide range of applications in neuromuscular research, and in the clinic.

The potential challenges to further scaling up the system to passive electrode arrays with higher density include:

- 1) The minimal pattern size of electrodes and serpentine wires ($\sim 10 \, \mu \text{m}$) that can be achieved in academic research laboratory by using conventional lithography and wet etching techniques.
- 2) Limited spaces for metal wires as they interconnect to the back-end data acquisition system.

The mechanical flexibility of the tattoo grid has been further assured during fabrication to meet the requirement of sEMG recordings, in which skin contours routinely change due to muscle contraction. Maintenance of stable signal recordings was a prominent limitation in earlier sEMG grid designs [2]. The new sEMG grid electrode designs shown here should be capable of stable signal recording, despite changes in the muscle shape and skin contours at different contraction levels.

To explore the stability of our signals during muscle contour deformation, we chose the biceps brachii, since this muscle displays a significant deformation of its shape because of muscle bulging during contraction, as reported earlier [31]. In our evaluations of the tattoo, the electrode grid contact and signal quality were not affected by muscle contour changes during an isometric contraction of the biceps brachii in the force range between 0% and 60%. The mean value of the signal activity to baseline ratio of the signal was above 30, which is comparable to the values obtained from the commercial grid electrodes (TMSI).

The advanced performance of the tattoo electrode was observed in the quality of the recorded signal. sEMG signal amplitudes were found to be significantly higher compared to a conventional commercial electrode of a similar size and layout (Fig. 6(a), (b) and Fig. 7(a), (b)). Propagation of the action potentials along the individual muscle fibers was recorded in the grid columns, highlighting the capacity for each electrode to record unique motor unit signals (Fig. 8). Furthermore, the frequency domain comparison of the sEMG signal confirms the frequency spectrum to be spread across the whole bandwidth of interest, with a significantly higher power across all recorded frequencies (as summarized in Table I). We observed a higher spectral content of the tattoo recording even at rest. This may be induced by the physiological noise present in the sEMG during the rest. This physiological noise is likely due to the low level motor unit discharge from the primary muscle (biceps brachii) and potentially from adjacent muscles (brachialis, coracobrachialis etc. in this case).

We believe that the higher power was obtained largely because of the higher amplitude of the recorded signal (Fig. 6(a)). This belief was substantiated by the larger peaks detected during the peak distribution analysis. Distributions of the peaks represent the population of detectable motor units during the muscle contraction. Distribution of peaks has been used in several motor unit studies [32], [33] and has been extended as a part of the sEMG studies [27]. The larger peaks are potentially attributable to the precise skin conformity of the electrode: due primarily to the soft silicone adhesive layer and to the compliant nature of the tattoo. A firm contact in such cases has been reported to reduce the impedance by 80% in an earlier study [34]. Despite the finding that peaks were much larger in the tattoo electrode recordings, the shapes of the peak distributions were preserved in comparison with the peak distribution derived from the commercial grid recordings (Fig. 7(a)) at matched contraction levels. This corroboration of peak distribution shape along with the bode amplitude response (Fig. 2(b)) assures that the signal was likely free from amplitude distortion during high-force muscle contraction.

The demonstrably faithful quality of the recorded signal was likely facilitated by the use of a matched reference electrode (fabricated with the same material) that was used during the experiment, as suggested by earlier studies [35], [36]. Another key factor promoting a stable baseline and low background noise was likely to be the low electrode-skin impedance achieved with the tattoo electrode. Earlier studies have reported electrodeskin impedances of several hundreds of kilo-ohms when grid electrodes utilize conductive electrode gel/paste, however, such systems have been also reported to have 40 times higher skinelectrode impedance without the conductive gel layer [37]. It is also important to mention that the tattoo electrode is able to maintain a similar skin-electrode impedance without any conductive gel or electrode paste applied [11], [38]. Indeed, it is noteworthy that we were able to attain a low electrode-skin impedance for a dry tattoo electrode, when we compared its performance to that of other, earlier reported experimental systems with larger skin-electrode interface [39].

The advantages of a dry electrode system are multifold in this type of high-density tattoo grid design. Dry tattoo grids are potentially easier to place on the skin [2], [40]. It may not always be possible to assure a uniform, conformal contact with the skin contour using a conventional grid electrode [41]. In contrast, the tattoo electrode, having an additional adhesive layer, enhances robust electrode-skin contact. Furthermore, elimination of the gel/paste also makes the electrode free from the potential short circuit of electrodes through the gel/paste layer, especially during repeated muscle contractions. This dry tattoo electrode is potentially a major advance by facilitating miniaturization of inter-electrode distance, and enabling the fabrication of a denser grid for clinical and research applications.

A conformal electrode-skin attachment in a dry gel/paste less configuration is also physiologically appealing as a tool to interpret an sEMG signal recorded from a muscle. The muscle bulging during the contraction induces amplitude and phase distortions of the MUAP's, which can be difficult to assess [42], [3]. The tattoo electrode, in contrast, has a remarkable flexibility of 60% which is an order of magnitude higher than that of the commercially available electrodes [8]. This flexibility allows the conformal skin interface to be preserved. The tattoo electrode also comes with extremely low bending stiffness that allows more secure attachment of the dry tattoo grid with the skin, even at small sizes [19], [18]. The thin flexible layer of silicone (65 μ m) preserves the electrode-skin interface environment, while it also offers enough peel adhesion to maintain robust skin conformity compared to the commercial grid. Better skin conformity has been reported to result signal recordings with better SNR in earlier studies [43]. The bilayer structure, the ultrathin external facing layer serves to protect the surrounding environment of the interface which improves the signal quality as demonstrated earlier [44].

The programmable features of the grid layout, including the electrode size and the inter-electrode distance of this tattoo electrode, together with easy wearability and faithful sEMG recording will potentially offer a considerable advantage and open new avenues in clinical research. One such application is following the natural history of severe neuromuscular disorders such as SMA or ALS which likely require prolonged tracking of the affected muscle(s) [1]. Reconfigurable layout and IED will also offer better discrimination of MU with optimal tattoo grid shape and size that was not possible with earlier grid electrodes.

VI. CONCLUSION

A flexible high-density tattoo electrode for HD-sEMG recording with programmable layout, built on stretchable electronics technology was developed, demonstrated and prototyped. We were able to record sEMG without perceptible distortion imposed by the electrode shapes and size. The tattoo electrode was used on intact human subjects during resting conditions with the muscle in a passive condition, and also during strong isometric contractions. Both active and resting phases were clearly visible in the recorded signal. The recorded sEMG signals have significantly larger amplitudes (p < .001) with a similar distribution shape of the peaks during the contractions. When compared to the recording obtained by a commercially available electrode. The experimental grid recordings had a better signal to noise ratio (>30) despite being dry in nature and despite minimal extra skin preparation. A major advantage offered by the electrode was the exceptional skin conformity; we were able to record from all the channels successfully during strong muscle contractions. We believe that the prototyped dry tattoo HD-sEMG grid represents a potentially important technological advance for potential clinical use of long-term HD-sEMG recording.

REFERENCES

- G. Drost et al., "Clinical applications of high-density surface EMG: A systematic review," J. Electromyogr. Kinesiol., vol. 16, no. 6, pp. 586–602, 2006
- [2] L. Inzelberg et al., "A wearable high-resolution facial electromyography for long term recordings in freely behaving humans," Sci. Rep., vol. 8, no. 1, pp. 1–9, 2018.
- [3] F. Negro et al., "Multi-channel intramuscular and surface EMG decomposition by convolutive blind source separation," J. Neural Eng., vol. 13, no. 2, 2016, Art. no. 026027.
- [4] J. Navallas, J. Rodriguez-Falces, and A. Malanda, "Inter-discharge interval distribution of motor unit firing patterns with detection errors," *IEEE Trans. Neural Syst. Rehabil. Eng.*, vol. 23, no. 2, pp. 297–307, Mar. 2015.
- [5] J. Rodriguez-Falces et al., "Spatial distribution of surface action potentials generated by individual motor units in the human biceps brachii muscle," J. Electromyogr. Kinesiol., vol. 23, no. 4, pp. 766–777, 2013.
- [6] S. Balasubramanian et al., "Is EMG a viable alternative to BCI for detecting movement intention in severe stroke?" *IEEE Trans. Biomed. Eng.*, vol. 65, no. 12, pp. 2790–2797, Dec. 2018.
- [7] D. F. Stegeman *et al.*, "High-density surface EMG: Techniques and applications at a motor unit level," *Biocybern. Biomed. Eng.*, vol. 32, no. 3, pp. 3–27, 2013.
- [8] B. G. Lapatki et al., "A thin, flexible multielectrode grid for high-density surface EMG," J. Appl. Physiol., vol. 96, no. 1, pp. 327–336, 2004.
- [9] P. Zhou et al., "Duration of observation required in detecting fasciculation potentials in amyotrophic lateral sclerosis using high-density surface EMG," J. Neuroeng. Rehabil., vol. 9, no. 78, 2012.
- [10] M. Hakonen, H. Piitulainen, and A. Visala, "Current state of digital signal processing in myoelectric interfaces and related applications," *Biomed. Signal Process. Control*, vol. 18, pp. 334–359, 2015.
- [11] L. Tian et al., "Large-area MRI-compatible epidermal electronic interfaces for prosthetic control and cognitive monitoring," Nat. Biomed. Eng., vol. 3, no. 3, pp. 194–205, 2019.
- [12] L. Bareket *et al.*, "Temporary-tattoo for long-term high fidelity biopotential recordings," *Sci. Rep.*, vol. 6, May 2016, Art. no. 25727.
- [13] B. Afsharipour et al., "Variations of tendon tap force threshold needed to evoke surface electromyogram responses after botulinum toxin injection in chronic stroke survivors," in Proc. 9th Int. IEEE/EMBS Conf. Neural Eng., San Francisco, CA, USA, 2019, pp. 385–388, doi: 10.1109/NER.2019.8717098.
- [14] S. C. Wang, K. S. Chang, and C. J. Yuan, "Enhancement of electrochemical properties of screen-printed carbon electrodes by oxygen plasma treatment," *Electrochim. Acta*, vol. 54, no. 21, pp. 4937–4943, 2009.
- [15] X. Wang et al., "Electrical and mechanical properties of ink printed composite electrodes on plastic substrates," Appl. Sci., vol. 8, no. 11, 2018, Art. no. 2101.
- [16] L. Pan et al., "Improving robustness against electrode shift of high density EMG for myoelectric control through common spatial patterns," J. Neuroeng. Rehabil., vol. 12, no. 1, pp. 1–16, 2015.
- [17] B. Afsharipour, S. Soedirdjo, and R. Merletti, "Two-dimensional surface EMG: The effects of electrode size, interelectrode distance and image truncation," *Biomed. Signal Process. Control*, vol. 49, pp. 298–307, 2019.
- [18] J. A. Rogers, T. Someya, and Y. Huang, "Materials and mechanics for stretchable electronics," *Science*, vol. 327, no. 5973, pp. 1603–1607, 2010.
- [19] J. J. S. Norton *et al.*, "Soft, curved electrode systems capable of integration on the auricle as a persistent brain–computer interface," in *Proc. Nat. Acad. Sci.*, vol. 112, no. 13, pp. 3920–3925, 2015.
- [20] S. L. Kappel et al., "Dry-contact electrode ear-EEG," IEEE Trans. Biomed. Eng., vol. 66, no. 1, pp. 150–158, Jan. 2019.
- [21] C. J. de Luca, "Surface electromyography: Detection and recording," DelSys Incorporated, pp. 1–10, 2002.
- [22] A. Bosnjak et al., "Performance assessment of dry electrodes for wearable long term cardiac rhythm monitoring: Skin-electrode impedance spectroscopy," in Proc. Annu. Int. Conf. IEEE Eng. Med. Biol. Soc. EMBS, 2017, pp. 1861–1864.

- [23] A. Miyamoto et al., "Inflammation-free, gas-permeable, lightweight, stretchable on-skin electronics with nanomeshes," Nat. Nanotechnol., vol. 12, no. 9, pp. 907–913, 2017.
- [24] B. Afsharipour *et al.*, "Spatial distribution of surface EMG on trapezius and lumbar muscles of violin and cello players in single note playing," *J. Electromyogr. Kinesiol.*, vol. 31, pp. 144–153, 2016.
- [25] A. Botter and R. Merletti, "A new method for the reduction of power line interference from multichannel bioelectric recordings," in *Proc. 2nd Congr. Nazionale di Bioingegneria*, Turin, Italy, Jul. 2010. [Online]. Available: http://hdl.handle.net/11583/2504626
- [26] B. Afsharipour, K. Ullah, and R. Merletti, "Amplitude indicators and spatial aliasing in high density surface electromyography recordings," *Biomed. Signal Process. Control*, vol. 22, pp. 170–179, 2015.
- [27] X. Li *et al.*, "Alterations in the peak amplitude distribution of the surface electromyogram poststroke," *IEEE Trans. Biomed. Eng.*, vol. 60, no. 3, pp. 845–852, Mar. 2013.
- [28] G. C. Agarwal and G. L. Gottlieb, "An analysis of the electromyogram by fourier, simulation and experimental techniques," *IEEE Trans. Biomed. Eng.*, vol. 22, no. 3, pp. 225–229, May 1975.
- [29] X. Li *et al.*, "Alterations in the peak amplitude distribution of the surface electromyogram poststroke," vol. 60, no. 3, pp. 845–852, 2013.
- [30] B. Afsharipour et al., "Using surface electromyography to detect changes in innervation zones pattern after human cervical spinal cord injury," in Proc. 38th Annu. Int. Conf. IEEE Eng. Med. Biol. Soc., 2016, pp. 3757–3760.
- [31] M. Al Harrach *et al.*, "Estimation of the relationship between external biceps brachii deformation and isometric contraction level using motion capture technique," in *Proc. XIV Mediterranean Conf. Medical Biolog. Eng. Comput.*, 2016, pp. 37–41.
- [32] M. Nikolic and C. Krarup, "Challenges in computerized MUAP analysis," in *Supplements Clin. Neurophysiol.*, vol. 60, X. Kong, Z. Han, and S. N. Gozani, Eds. 2009, pp. 97–103.
- [33] L. McManus *et al.*, "Changes in motor unit behavior following isometric fatigue of the first dorsal interosseous muscle," *J. Neurophysiol.*, vol. 113, no. 9, pp. 3186–3196, 2015.
- [34] G. Li, S. Wang, and Y. Y. Duan, "Towards conductive-gel-free electrodes: Understanding the wet electrode, semi-dry electrode and dry electrode-skin interface impedance using electrochemical impedance spectroscopy fitting," Sensors Actuators, B Chem., vol. 277, pp. 250–260, Dec. 2018.
- [35] E. S. Kappenman and S. J. Luck, "The effects of electrode impedance on data quality and statistical significance in ERP recordings," *Bone*, vol. 23, no. 1, pp. 1–7, 2008.
- [36] A. Albulbul, "Evaluating major electrode types for idle biological signal measurements for modern medical technology," *Bioengineering*, vol. 3, no. 3, pp. 20, 2016.
- [37] B. G. Lapatki et al., "A thin, flexible multielectrode grid for high-density surface EMG," J. Appl. Physiol., vol. 96, no. 1, pp. 327–336, 2004.
- [38] A. A. Chlaihawi *et al.*, "Development of printed and flexible dry ECG electrodes," *Sens. Bio-Sensing Res.*, vol. 20, no. March, pp. 9–15, 2018
- [39] P. Fayyaz Shahandashti et al., "Highly conformable stretchable dry electrodes based on inexpensive flex substrate for long-term biopotential (EMG/ECG) monitoring," Sensors Actuators, A Phys., vol. 295, pp. 678–686, Aug. 2019.
- [40] P. Laferriere, E. D. Lemaire, and A. D. C. Chan, "Surface electromyographic signals using dry electrodes," *IEEE Trans. Instrum. Meas.*, vol. 60, no. 10, pp. 3259–3268, Oct. 2011.
- [41] L. G. Wiedemann and A. J. McDaid, "On the function and robustness of skin-electrode interfaces for high-density electromyography: Towards ubiquitous integration with robotics devices," in *Proc. IEEE Life Sci. Conf.*, 2018, pp. 137–140.
- [42] A. Holobar et al., "Experimental analysis of accuracy in the identification of motor unit spike trains from high-density surface EMG," *IEEE Trans. Neural Syst. Rehabil. Eng.*, vol. 18, no. 3, pp. 221–229, Feb. 2010.
- [43] P. A. Lopes *et al.*, "Soft bioelectronic stickers: Selection and evaluation of skin-interfacing electrodes," *Adv. Healthcare Mater.*, vol. 8, no. 15, pp. 1–11, 2019.
- [44] P. Cattarello and R. Merletti, "Characterization of dry and wet electrodeskin interfaces on different skin treatments for HDsEMG," in *Proc. IEEE Int. Symp. Med. Meas. Appl.*, Benevento, Italy, 2016, pp. 1–6, doi: 10.1109/MeMeA.2016.7533808.